Fatigue behaviour of Nitinol peripheral stents: The role of plaque shape studied with computational structural analyses

Elena Dordoni [a], Alessio Meoli [a], Wei Wu [a], Gabriele Dubini [a], Francesco Migliavacca [a], Giancarlo Pennati [a], Lorenza Petrini [b,*]

[a] *Laboratory of Biological Structure Mechanics, Department of Chemistry, Materials and Chemical Engineering 'Giulio Natta', Politecnico di Milano, Italy*
[b] *Department of Civil and Environmental Engineering, Politecnico di Milano, Italy*

Received 10 September 2013
Received in revised form 13 March 2014
Accepted 15 March 2014

1. Introduction

Peripheral arterial disease (PAD) is one of the major manifestations of systemic atherosclerosis: it involves the presence of a partial or total occlusion of peripheral arteries due to plaque formation, resulting in a progressive impairment of the distal vasculature. Anatomically, most of these lesions are located in the lower limb arteries downstream from the renal arteries, with more than 50% of all PAD cases involving the superficial femoral artery (SFA) and the popliteal artery (PA) [1].

In the last decades endovascular procedures have become more and more popular with respect to surgical intervention, thanks to their reduced impact on the patient life and their limited cost for the national health systems. In particular, nowadays the placement of self-expandable Nitinol stents, after percutaneous transluminal angioplasty (PTA), is the preferred technique for the treatment of PAD. A number of clinical studies [2–4] reported high rates of technical success of the stenting procedure and higher vessel patency rates in the medium to long-term follow-up than those obtained with PTA alone.

Self-expandable stents exploit the Nitinol pseudo-elastic property. From the procedural point of view, stents are manufactured in an open configuration with a diameter slightly larger than the lumen of the target vessel. The ratio between the external diameter of the stent in the open configuration and the inner diameter of the stenotic vessel is defined as *oversizing*. Stents are radially compressed (crimping) to allow their insertion into a retractable sheath placed on a guide catheter. Finally, at the treatment site, they self-expand while the sheath is gradually withdrawn. After the placement in the stenotic zone, pseudo-elasticity provides the stent with a high conformability to the vessel morphology, a high flexibility and a capability to recover the initial shape during cyclic loads. Despite all these features making Nitinol stents ideal for the application of interest, the effectiveness of SFA stenting is still undermined by clinical complications related to the fatigue failure of these devices. Different studies [5–7] reported various fracture rates of stents implanted in the SFA-PA, ranging between 14 and

* Corresponding author at: Laboratory of Biological Structure Mechanics, Civil and Environmental Engineering Department, Politecnico di Milano, Piazza Leonardo da Vinci 32, 20133 Milan, Italy. Tel.: +39 0223994316; fax: +39 0223994286.
E-mail address: lorenza.petrini@polimi.it (L. Petrini).

24.5%, often associated with in-stent restenosis and failure of the stenting procedure.

The unique biomechanical environment of this district appears as the main factor for the high incidence of stent fracture. Indeed, hip and knee joint movements associated with patients daily activities expose the artery, and therefore the implanted stent, to repetitive cyclic loadings including axial compression, bending and torsion [8–10] that could lead to long-term failure of the device.

Since the fatigue fracture of Nitinol stents implanted into the femoro-popliteal district represents a critical clinical issue, it is interesting to investigate the mechanical response of these devices, to understand their fatigue behaviour and to gain useful information for the design of stents with higher mechanical reliability.

Nowadays, numerical studies on the performance of femoro-popliteal Nitinol stents – mostly based on finite element analyses (FEA) – are already available in the literature [11–15]. However, those considering the stent fatigue failure disregard the presence of an atherosclerotic plaque [11–13], even if PAD is often characterized by long and diffuse lesions, with frequent, distributed occlusions [1,16,17]. On the contrary, studies considering the plaque presence do not consider cyclic loading conditions [14,15]. From the experimental side, there are two recent papers devoted to the study of fatigue in peripheral Nitinol stents. Müller-Hülsbeck et al. [18] compared the performance of different marketed devices, but they did not apply physiological cyclic loading conditions; those authors only tested stents in their fully-expanded configuration, neglecting the stent–vessel interaction. Nikanorov et al. [19] carried out axial compression and bending tests on stents after their deployment in a silicone tube; they were able to reproduce the presence of the femoral artery (without plaque) and the applied loads were consistent with *in vivo* ranges of deformation of the literature [8,20]. In the paper by Meoli et al. [13], where FEA were used to investigate the fatigue testing conditions adopted in the two *in vitro* studies cited above, the authors showed that stent-to-tube oversizing ratio plays an important role in determining the fatigue response of Nitinol stents. However, the vessel was simulated as a tube with uniform thickness. What currently remains unclear is the influence of the plaque shape on the reaction of the stent to the cyclic loading. To clarify this point, the present paper proposes a procedure based on FEA to study the stent fatigue behaviour through the development of different stenotic vessel models subjected to cyclic axial compression and bending after angioplasty and stenting. For each condition, mean and alternate strains are calculated and compared using the Constant Life Diagram. The definition of the most dangerous condition would require the comparison of the results with the Nitinol fatigue strain limit curve for a number of cycles $N = 10^7$ corresponding to 10 years of gait [18]. The limit curve should be experimentally built by performing fatigue tests on the real stent material, because the results of these tests are dependent on the specific material properties and thermo-mechanical treatments (laser cut and surface processing). However, researchers usually refer to the curve proposed by Pelton et al. [21] adding a number of simplifications. In some cases [11,12] the alternating strain is considered constant (0.4%) independently from the mean strain value; in other cases [22] the alternating strain is assumed constant (0.4%) only among 0% and 1.5% of mean strain, while it increases with almost constant slope of 0,133 between 1.5% and 4% of mean strain (Fig. 1). In this paper considerations on Nitinol fatigue strain limit curves and device fatigue life are also reported and discussed.

2. Methods

Finite element analyses were used to simulate the deployment of a self-expandable Nitinol stent in a peripheral artery and the subsequent *in vivo* loading conditions. The commercial finite element code ANSYS Mechanical APDL 14.0 (Ansys Inc., Canonsburg, PA, USA) was used to run the simulations.

A 3D stent model resembling the geometry of a commercial peripheral stent from Invatec (now Medtronic Endovascular Therapies, Roncadelle, BS, Italy) was built with the aid of the software Pro/ENGINEER Wildfire 4.0 (Parametric Technology Corporation), starting from images acquired by a stereo microscope Nikon SMZ800 (Nikon Corporation, Tokyo, Japan). The stent in the open configuration has an external diameter of 8 mm, a length of 45.8 mm and a strut thickness of 0.17 mm. The device is made by Nitinol, whose pseudo-elastic behaviour was described through the Shape Memory Alloy (SMA) material model already implemented in the ANSYS code. The non-linear mechanical input properties for the SMA material model were derived from uniaxial tension tests performed on Nitinol samples. The samples were cut by laser from the same tubes used to produce the stents under study and subjected to the same treatments, according to the methodology presented in Petrini et al. [23]. The value of the parameters used by the ANSYS constitutive model to take into account the tension-compression asymmetry observed in Nitinol [24–26], was set equal

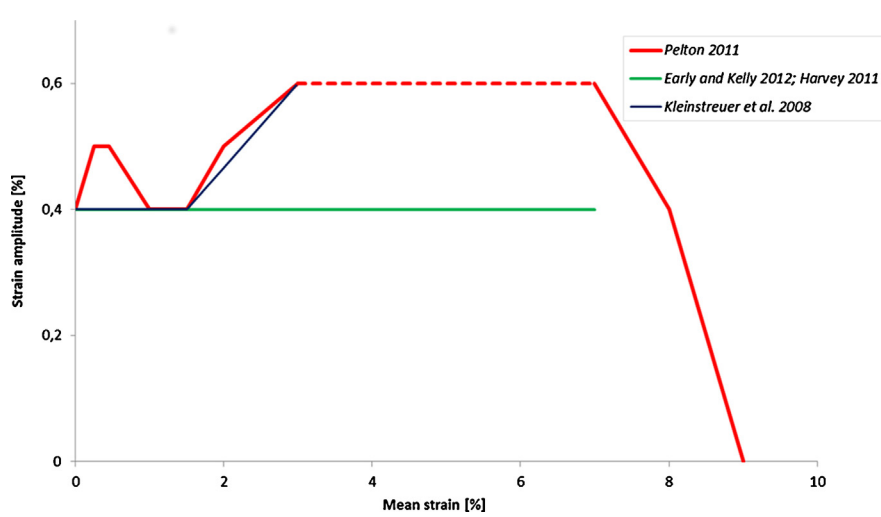

Fig. 1. Nitinol fatigue strain limit curves at $N = 10^7$ cycles found in literature. The red line is the limit proposed by Pelton [21], based on experimental fatigue tests on Nitinol specimens; the green and blue lines are simplification of the previous one, showed by Early and Kelly [11], Harvey [12], and Kleinstreuer [22]. (For interpretation of the references to colour in this figure legend, the reader is referred to the web version of the article.)

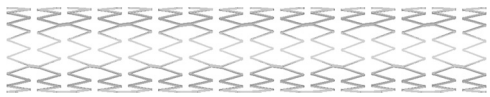

Fig. 2. 3D CAD model of the peripheral stent, which consists of open cell design, peak to peak connections and three links for each crown.

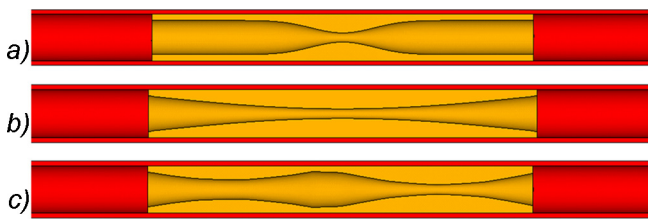

Fig. 3. Stenotic vessel models having: (a) plaque with high sharpness, (b) plaque with low sharpness and (c) plaque with a double peak and low sharpness.

to 0.19 according to literature [15,27,28]. This because experimental data related to the behaviour of the material in compression are unavailable. The reconstructed CAD model of the peripheral stent is depicted in Fig. 2.

A model of the stenotic vessel, distinguishing between artery and plaque, was developed. The considered distal SFA-proximal PA segment was modelled as a hollow cylinder with an inner diameter of 5.6 mm, a thickness of 0.56 mm and a length of 100 mm. The plaque shape was modelled according to the Hicks–Henne function [29] reported in Eq. (1):

$$y = \frac{D_V}{2} \times (1 - RS) \times \sin\left(\pi \times \frac{x}{L_P}\right)^s \quad (1)$$

This function is described by four parameters: D_V (vessel inner diameter), RS (residual stenosis), L_P (plaque length) and S (sharpness of the peak). Three models of vessels were built with concentric plaques having the same maximum RS (80% of the healthy vessel lumen) and L_P (45.8 mm), but different sharpness and number of stenoses: (i) a plaque with high sharpness (Fig. 3a), (ii) a plaque with low sharpness (Fig. 3b), and (iii) a plaque with a double peak and low sharpness (Fig. 3c). The non-linear behaviour of the artery was described with a hyperelastic isotropic Mooney–Rivlin constitutive law based on a third-order polynomial strain energy density function, with parameters derived from experimental tests on human femoral artery specimens [30]. The plaque was modelled with an elasto-plastic material to take into account, in a simplified way, the plaque fracture after PTA: in the absence of specific bibliographic data on femoro-popliteal plaques, the yielding point of 270 kPa was identified from experimental data of tensile tests on samples of atherosclerotic aortic plaques [31]. Both the stent and the stenotic vessel models were meshed using 8-node cubic elements (SOLID185) with full integration algorithm. A sensitivity analysis was performed to ensure a proper mesh refinement, considering a simplified model with one stent ring and the corresponding portion of the artery–plaque system. The parameters chosen to compare the sensitivity analysis results were the maximum radial displacement of the vessel after the deployment of the device and the first principal strain in the stent. The analysis was run varying the ratio between the vessel and the stent element number, keeping constant the number of stent elements. Three different ratios were considered: 0.1, 0.5, and 1 (upper panel of Fig. 4). The finest mesh of the vessel gave a more accurate description of the displacement field, however the difference observed in the three cases in terms of maximum values was not significant (U_r in the lower panel of Fig. 4). Moreover, since the fatigue response of the stent is related with the tensile strain, we focused on the first principal strain field through the device after its deployment and we found that its value was the same in the three cases (ε^1_{tot} in the lower panel of Fig. 4). Therefore, a ratio of 0.1 was chosen representing the best balance between acceptable calculation time and results accuracy.

The simulated loading steps were:

- PTA: to reproduce the stress/strain field in the stenotic vessel before stenting.
- Crimping of the stent inside a sheath: to reproduce the stress/strain field in the stent before the self-expansion.

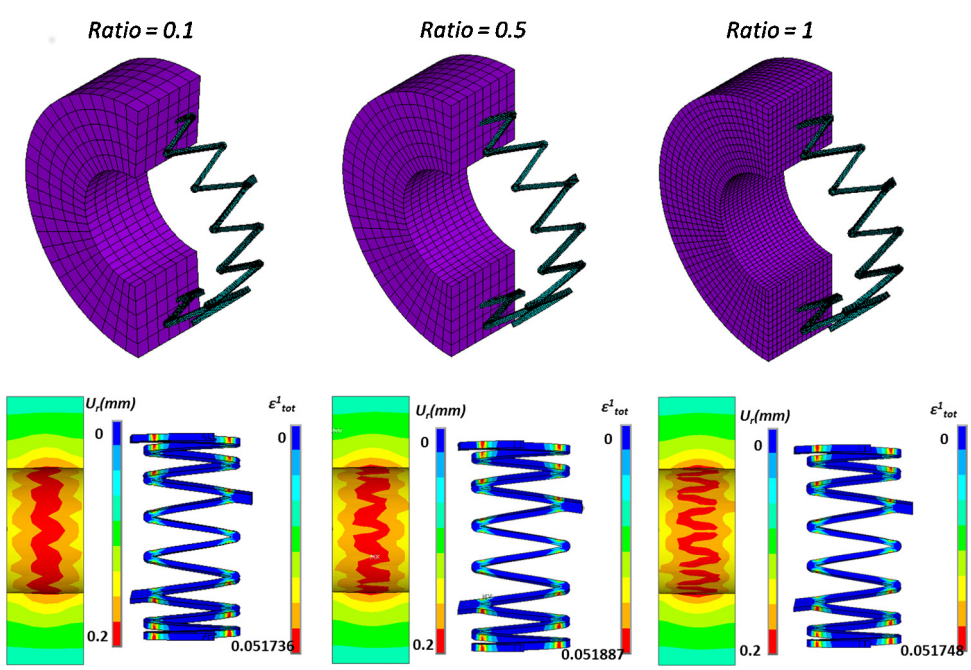

Fig. 4. Three different ratios between stenotic vessel and stent elements in a simplified model (above) and corresponding results in terms of wall radial displacement (U_r) and first principal strain (ε^1_{tot}) through the stent (below).

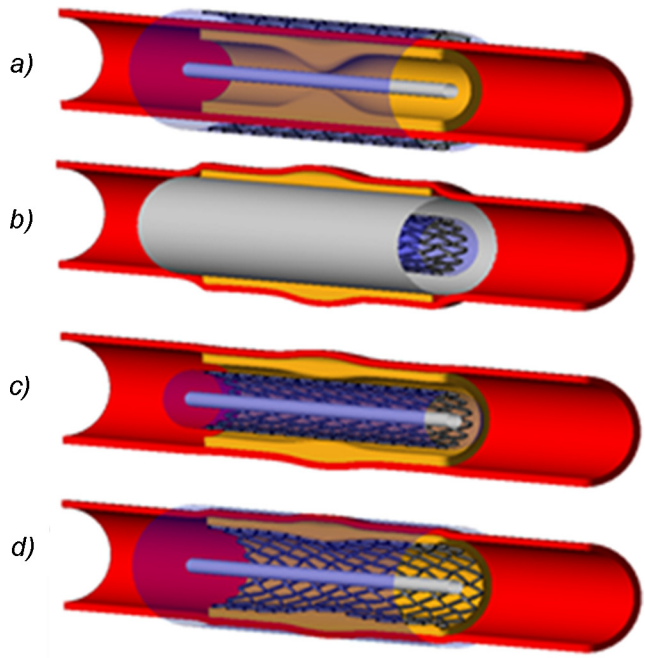

Fig. 5. Stenting procedure: (a) initial configuration, (b) end of stent crimping and expansion of the angioplasty balloon, (c) after the release of the angioplasty balloon and (d) after the stent self-expansion.

- Self-expansion of the stent: to reproduce the equilibrium condition between the stent and the vessel radial force.
- Physiological cyclic axial compression and bending of the vessel: to analyse the stent fatigue behaviour.

The boundary conditions applied are described in the following.

PTA required the simulation of the balloon inflation. This was obtained with a cylindrical rigid surface, placed along the centreline of the vessel (Fig. 5a) and then expanded in the radial direction (Fig. 5b). A flexible–rigid contact pair between the balloon and the plaque inner surface was defined. The balloon nodes were moved up to reach a diameter equal to 1.1 times the vessel inner diameter: this value was chosen to ensure the achievement of a *RS* lower than 30% that is the condition required by clinicians for continuing with the stenting procedure. At the end of this step, the balloon was deflated, allowing the plaque and artery elastic recoil (Fig. 5c). The crimping of the stent was performed using a cylindrical rigid surface mimicking the sheath of the catheter (Fig. 5b). The rigid surface with an initial diameter 1% greater than the stent outer diameter and the same stent length was positioned coaxially with the stent. A flexible–rigid contact pair between the rigid surface and the stent outer surface was defined, while no contact was active between the rigid surface/stent and the vessel. The crimping was simulated by imposing a negative radial displacement to the nodes of the rigid surface up to a diameter that allowed the insertion of the stent into the stenotic vessel treated by angioplasty. In the subsequent step the stent was released into the vessel. The rigid surface was re-opened up to the initial position by imposing a positive radial displacement to the rigid body nodes. The stent, free to expand, can only partially recover its original open configuration: a flexible–flexible contact pair between the stent outer surface and the plaque inner surface was activated (Fig. 5d). An internal pressure, equal to the mean of the systolic and diastolic pressures, was applied at the inner surface of the artery–plaque system to reproduce the physiological blood pressure condition (Fig. 6a). To define the rigid surface – stent and stent – plaque contact pairs during stent deployment and cyclic loading simulations a friction coefficient was set according to the following considerations. During the

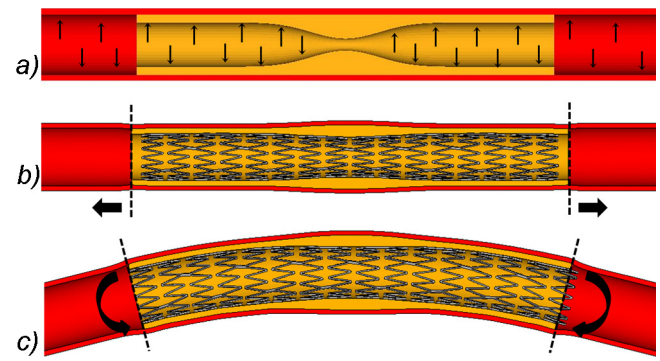

Fig. 6. Application of boundary conditions: (a) cyclic blood pressure, applied on the inner surface of the stenotic vessel, (b) cyclic axial compression, performed applying axial displacement at both vessel-plaque ends, after stent deployment and (c) cyclic bending obtained applying a rotation at both vessel-plaque ends, after stent deployment.

crimping of the stent, the friction coefficient is quite low due to the particular technique employed by the crimping machine commonly used by the companies (*MSI catheter and stent testing, RX 550/650, Machine Solutions, User Manual*). Regarding the contact definition during the stent self-expansion, to the authors' knowledge, no reference is available in the literature that attests the value of friction coefficient between Nitinol and atherosclerotic plaque. Hence, we based our choice on a sensitivity analysis in which we considered three different values for the coefficient at the interface between stent outer surface and cylindrical rigid body (crimping) and between stent outer surface and vessel (self-expansion) ranging from low to high friction: 0.02, 0.2 and 1. The results showed that the value of friction coefficient does not affect radial displacements and stent maximum principal strains. A value of 0.2 was selected in the whole simulation to minimize the computational time and maintain result accuracy. Moreover, a value of 0.2 was used by Yang et al. [32] for friction between steel and silicon and was also considered during *in vitro* fatigue tests on Nitinol stents deployed in silicon tubes [19,33].

After the stent placement into the vessel, cycling loading conditions of axial compression and bending were applied on SFA to mimic the *in vivo* environment. Three loading and unloading cycles were performed due to the material model implemented in ANSYS. In fact, when cycles are imposed to the material already deformed up to the plateau, the constitutive model response stabilizes after three loading cycles.

The values of axial and bending loads were defined within the range of deformation experienced *in vivo* according to the results of a study on cadavers [19]. In particular, a value of 5% was chosen for the stent cyclic axial compression corresponding to the average between the distal-SFA/proximal-PA and the PA strains during 70°/20° knee/hip flexion, that represents walking conditions; a bending angle of 28° was chosen, corresponding to a stent curvature of 0.0106 rad mm^{-1}, that represents an intermediate value for the curvature found in the PA during 70°/20° and 90°/90° knee/hip flexion.

The cyclic compression was performed by applying a displacement at both plaque ends. The vessel was axially stretched by 5% before the stent deployment, carried back to its original length after the device release and finally subjected to three cycles of deformation up to 5% and return to 0% (Fig. 6b). As a result of the contact friction between the stent outer surface and the plaque inner surface, the stent was subjected to cycles of axial shortening of about 5%.

The cyclic bending was performed at the end of the axial cycles, starting from the un-stretched configuration, by applying a rotation at both plaque ends in order to obtain a change in the curvature of

the artery–plaque system, and therefore a change in the curvature of the stent (Fig. 6c). The numerical results were analysed in terms of maximum principal strains in the stent [34] at each load-step. In particular, a user-defined script written in APDL language was developed for the calculation of mean (ε_m^1) and alternating (ε_a^1) first principal strain values that occur in each stent element in response to the application of a loading cycle. The following formulae were used (Eqs. (2) and (3)):

$$\varepsilon_m^1 = \left(\frac{\varepsilon_i^1 + \varepsilon_{(i+1)}^1}{2} \right) \tag{2}$$

$$\varepsilon_a^1 = \left(\frac{\varepsilon_i^1 + \varepsilon_{(i+1)}^1}{2} \right) \tag{3}$$

where i is the last sub-step of a generic load step and $i+1$ is the last sub-step of the following unload step. The results were plotted in a Constant Life Diagram and compared with the Nitinol fatigue strain limit curve. For the definition of the limit curve we referred to the results of fatigue tests performed by Pelton [21]. However, in order to take into account possible differences between our stent material and the material tested by Pelton, the fatigue limit was defined not with a single curve (ε_m^1, ε_a^1) but with a range of alternating strain values for a given mean strain value. Practically, the range is defined by a low limit curve and a high limit curve, while the curve proposed by Pelton [21] and plotted in Fig. 1 is considered the average limit curve. The risk of fatigue fracture for the stent can be low, mean, high or very high depending on the positions of the points (ε_m^1, ε_a^1) with respect to the limit curves (below the low limit curve, among the mean and the average limit curves, among the average and the high limit curves, above the high limit curve). In this work, a few fatigue experimental tests were performed on the same specimens used for the material mechanical characterization as reported in a previous paper of ours [23]: the results of those tests allowed the definition of an interval of amplitude ±0.1 around the average limit curve.

3. Results

The mean and alternating strain distributions in the stent caused by cyclic axial compression are reported in the form of contour maps in Fig. 7. The plaque shape considerably affects the strain distribution through the stent.

The mean strain distribution is mainly determined by the oversizing. The plaque shapes show similar mean strain value due to the equal stenosis rate in the undeformed configuration and after the PTA procedure. In particular, as shown in Fig. 7, the maximum value of the mean strain is equal to 5.3% and it is located in the *v-struts* positioned in proximity of the plaque peak, where the vessel inner diameter is smaller, while it decreases to 4.8% where the inner diameter increases. Moreover, the stent diameter reduction from the initial open configuration takes place with the closure of the *v-struts* that implies a bending solicitation in their apex. For that reason, the maximum mean strain value is located in this position at the end of stent self-expansion.

The alternating strain distribution is influenced by the thickness of the artery–plaque system, and therefore by its stiffness. The smaller the thickness, the greater the vessel shortening; the stent, due to the imposed friction, moves with the wall and consequently higher strains are generated in these regions. The maximum alternating strain values are located where the plaque exhibits a smaller thickness (and lower stiffness) and therefore the stent undergoes a higher compression. In the case of concentric plaque with high sharpness, the axial stiffness decreases from 2.07 N/mm in the peak zone to 1.26 N/mm in the lateral parts and the alternating strain value increases from 0.09% to 0.16%. In the case of concentric plaque with low sharpness, the axial stiffness decreases from 2.14 N/mm in the central zone with higher thickness to 1.75 N/mm in the lateral parts and the alternating strain value increases from 0.13% to 0.16%. Finally, in the case of plaque with double peak, the axial stiffness decreases from 2.21 N/mm where the plaque has a larger thickness to 1.51 N/mm in the central part and the alternating strain increases from 0.13% to 0.24%. In all the cases, the maximum values of alternating strain are located at the connection between *links* and *v-struts*. During axial compression, the stent accommodates the induced shortening by opening the angle of the *v-struts* connected with the links and rigidly rotating the *v-struts* not connected with the links.

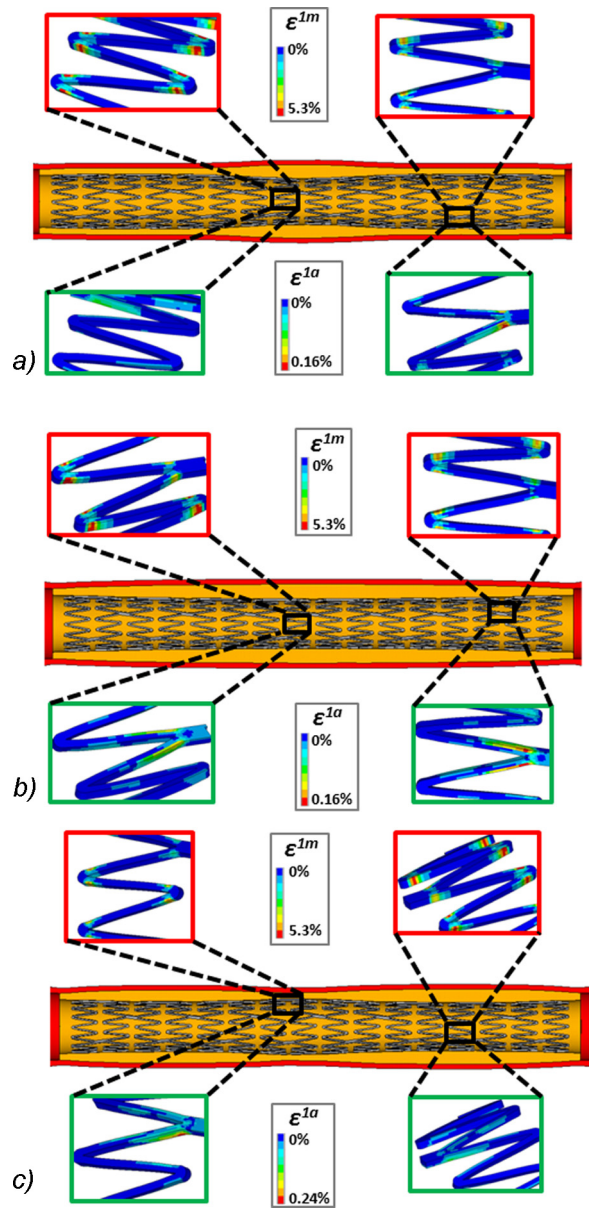

Fig. 7. Mean and alternating first principal strain contour maps for each plaque shape analysed in case of cyclic axial compression: (a) plaque with high sharpness, (b) plaque with low sharpness and (c) plaque with a double peak. In the red boxes, values of mean strain, while in green ones, values of alternating strain are reported. (For interpretation of the references to colour in this figure legend, the reader is referred to the web version of the article.)

In the case of bending (Fig. 8) the mean first principal strain distribution is very similar to the axial case in the three configurations,

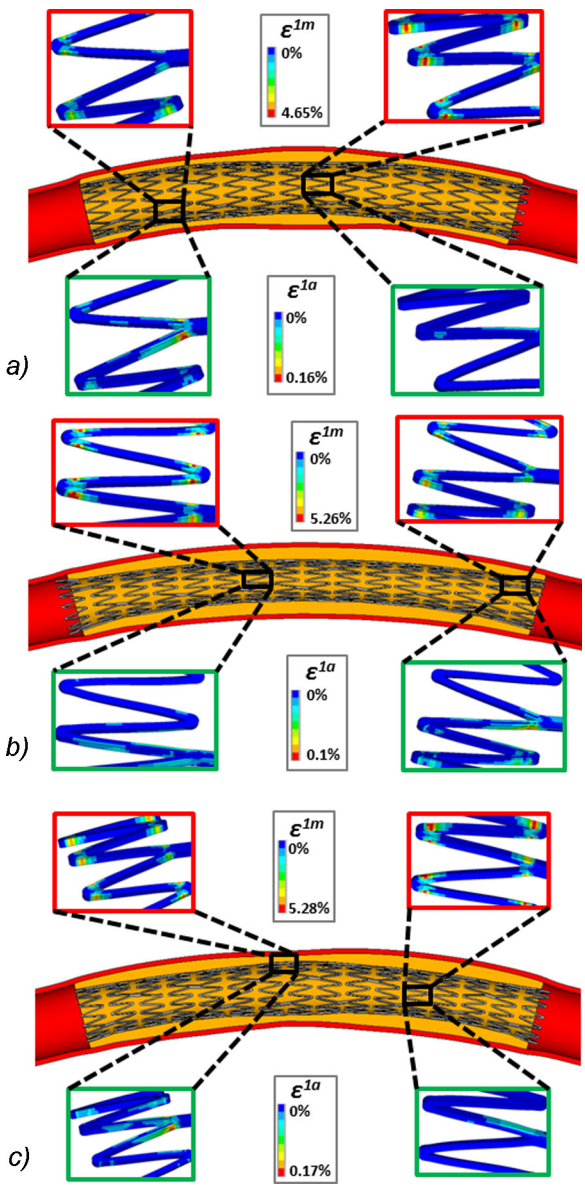

Fig. 8. Mean and alternating first principal strain contour maps for each plaque shape analysed in case of cyclic bending: (a) plaque with high sharpness, (b) plaque with low sharpness and (c) plaque with a double peak. In the red boxes, values of mean strain, while in green ones, values of alternating strain are reported. (For interpretation of the references to colour in this figure legend, the reader is referred to the web version of the article.)

even if the maximum values are slightly lower. This is due to the fact that during bending the pre-stretch was not taken into account; accordingly, the vessel enlarges its diameter and the stent oversizing decreases. In particular, this happens in the case of plaque with high sharpness because of a less uniform stiffness distribution of the artery–plaque system.

The alternating first principal strain is still maximum in the connections between *links* and *v-struts* and higher in the case of a double peak plaque. By comparing the maximum values due to the bending with those of the axial compression, they are lower for the configurations with low sharpness, while they reach the same maximum values in case of concentric plaque with high sharpness. In Figs. 9 and 10 the Constant Life Diagrams of the stent loaded under cyclic axial compression and bending for the three plaque shapes are compared with the *limit curves* of the material. It is interesting to notice how the distribution of the maximum alternating strain varies in the studied cases and the shape of the limit curve may influence the fatigue risk. Indeed, for the plaque with one peak and low sharpness during axial compression and bending and for the plaque with high sharpness during axial compression, the alternating strain reaches its maximum value in correspondence of a wide range of mean strains (from 1.5% to 3%). The double peak plaque during axial compression has maximum alternating strain when the mean strain is around 1%, while during bending the maximum alternating strain is shifted to a value of mean strain around 2.5%. The plaque with high sharpness has the maximum alternating strain when the mean strain is around 1.5%. The peculiar shape of the Nitinol fatigue limit indicates the double peak plaque for cyclic compression and the high sharpness plaque for the bending as the most dangerous cases because they produce maximum alternating strain in the zone of minimum of the curve. Clearly, simplifying the curve with a constant value of alternating strain [11,12] would have overestimated the risk for the other cases. Finally, the comparison with the limit curves shows that the stent is safe in all the studied cases, being the couples of mean and alternating strain values below the low limit curve. However, the double peak plaque configuration during cyclic axial compression can be considered the most critical condition because it gives the highest maximum alternating strain in correspondence of mean strain ranging between 1% and 1.5%.

4. Discussion

Numerical models are nowadays a widely recognized useful tool to study the interaction of the stent with tissues and organs [35]. Mechanical stent fracture due to cyclic loading is emerging as one of the critical issues for the stenting procedure success [36,37]. Clinical studies showed that factors such as stent design, vascular district properties and loading conditions are possible causes of stent fracture. In this study, a procedure based on finite element models is proposed to evaluate the influence of plaque morphologies on stent fatigue resistance under cyclic loading conditions mimicking SFA movements. The evaluation is based on the numerical results to build the Constant Life Diagrams in terms of mean and alternating first principal strains. Moreover, low and high fatigue strain limit curves at 10^7 cycles are taken into consideration. The peculiar shape of these two curves (Figs. 9 and 10) indicates that points with mean strain values smaller than 1.5% are the most dangerous: they correspond to the stent zones having a low oversizing. This implies that the plaque shape has a great influence on the alternating strain values. Indeed, its geometry (especially the thickness) remarkably affects the vessel local axial stiffness and also the way to transfer the load to the stent: artery–plaque zones with small thickness (low stiffness) can easily shorten or bend. As a consequence the corresponding stent zones have lower mean strains and higher alternating strains than those located where the artery–plaque thickness is higher. In particular, multiple lesions seem to be the most critical condition since the alternating strain values are higher than in the other plaque configurations, in both cases of cyclic axial compression and bending. Highest deformations are concentrated between the two stenoses, where the stiffness of the vessel is lower. This result suggests the use of multiple stents to cover a double-peak plaque, instead of a single, long stent that might be subjected to high deformation between the two stenoses. Moreover, this finding explain why longer stents are more prone to fatigue fracture than shorter ones [5–7]: the longer the stent, the higher is the probability of treating also safe vessel zones (without plaque). The low stiffness of these zones induces high strains in the stent, and hence the risk of fracture increases.

For all the plaque configurations examined, the stent is more prone to fracture under axial compression than bending: axial

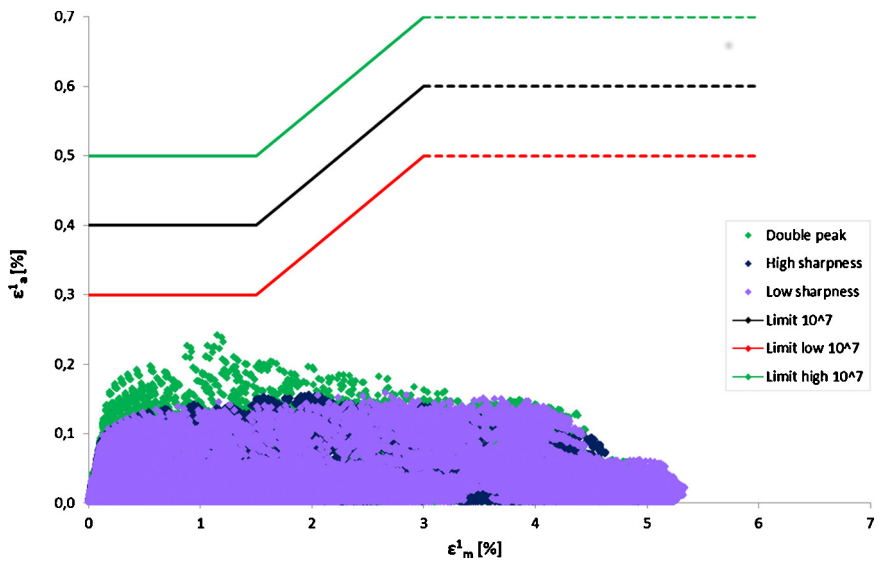

Fig. 9. Constant Life Diagram for cyclic axial compression. Couples of values $(\varepsilon_m^1; \varepsilon_a^1)$ for the three plaque shapes are reported and compared with the fatigue strain limits at 10^7 cycles: the red line represents the low fatigue limit, the green one the high fatigue limit, while the black, according to literature data [21], is considered the average limit curve. (For interpretation of the references to colour in this figure legend, the reader is referred to the web version of the article.)

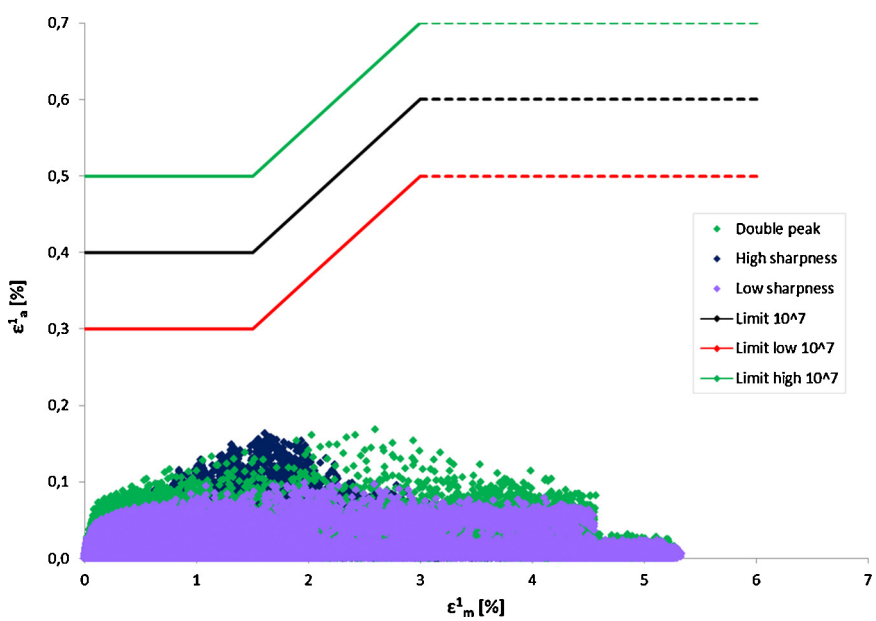

Fig. 10. Constant Life Diagram for cyclic bending. Couples of values $(\varepsilon_m^1; \varepsilon_a^1)$ for the three plaque shapes are reported and compared with the fatigue strain limits at 10^7 cycles, distinguishing between low, high and average fatigue limits [21].

compression is the most critical loading condition for the distal SFA-proximal PA. This final remark is in agreement with the study by Early and Kelly [11].

5. Limitations

A limitation of this study is the use of simplified material models for the plaque and the artery. Our simplified models may fail to provide an accurate prediction of the vessel stresses following stent implantation; however, they can be considered reasonably valid when comparing the stent strain distributions in the different studied cases. To the purpose, more sophisticated arterial model can be adopted taking into account the different arterial layers with the mechanical properties measured on SFA samples, as proposed by Holzapfel et al. [38] on coronary arteries. Regarding the plaque, the presence of microcalcifications as recently proposed by Kelly-Arnold et al. [39] can be a further step for a better mechanical description of the vessel behaviour and the response of the stent performances. Moreover, also the cylindrical geometry of the artery could be considered as an additional limitation, since it is not representative of a patient-specific vessel; however, the purpose of the authors was the description of the effect of the plaque shape on the fatigue resistance of the implanted device. This stands also for simplified geometries.

The adopted criterion for estimating the fatigue life of the stent, based on the use of the first principal strain as index of risk, is a questionable choice, although it is the most common in the literature [8,11]. Since the stent is subject to a multi-axial state of solicitations, a further development of our model is the implementation of a fatigue criterion with an equivalent mean and alternate strain, taking into account other components of the strain [12,40].

In this work the proposed numerical procedure is applied only to a single, specific stent. This might limit the validity of our conclusions that should be tested also for different device designs.

In general, we believe that these limitations do not affect the main achievement of this study, *i.e.* a methodology based on finite element simulations to evaluate the influence of plaque geometry on the stent fatigue behaviour.

Our next step will be to validate the proposed FEA approach performing dedicated bench tests.

Funding

This work is within the project "RT3S – Real Time Simulation for Safe vascular Stenting" partially funded by the European Commission under the 7th Framework Programme, GA FP7-2009-ICT-4-248801.

Ethical approval

Not required.

Conflict of interest

None declared.

References

[1] Zeller T. Current state of endovascular treatment of femoro-popliteal artery disease. Vasc Med 2007;12:223–34.
[2] Krankenberg H, Schlüter M, Steinkamp H, Bürgelin K, Scheinert D, Schulte KL. Nitinol stent implantation versus percutaneous transluminal angioplasty in superficial femoral artery lesions up to 10 cm in length: the Femoral Artery Stenting Trial (FAST). Circulation 2007;116:285–92.
[3] Laird JR, Katzen BT, Scheinert D, Lammer J, Carpenter J, Buchbinder M. Nitinol stent implantation versus balloon angioplasty for lesions in the superficial femoral artery and proximal popliteal artery. Twelve-month results from the RESILIENT randomized trial. Circ Cardiovasc Interv 2010;3(3):267–76.
[4] Schillinger M, Sabeti S, Loewe C, Dick P, Amighi J, Mlekusch W, et al. Balloon angioplasty versus implantation of Nitinol stents in the superficial femoral artery. N Engl J Med 2006;354:1879–88.
[5] Allie DE, Hebert CJ, Walker CM. Nitinol stent fracture in the SFA. Endovasc Today 2004;7:22–34.
[6] Scheinert D, Scheinert S, Sax J, Piorkowski C, Braunlich S, Ulrich M, et al. Prevalence and clinical impact of stent fractures after femoropopliteal stenting. J Am Coll Cardiol 2005;45(2):312–5.
[7] Iida O, Nanto S, Uematsu M, Ikeoka K, Okamoto S. Influence of stent fracture on the long-term patency in the femoro-popliteal artery: experience of 4 years. JACC Cardiovasc Interv 2009;2:665–71.
[8] Klein AJ, Chen SJ, Messenger JC, Hansgen AR, Plomondon ME, Carroll JD, et al. Quantitative assessment of the conformational change in the femoropopliteal artery with the leg movement. Catheter Cardiovasc Interv 2009;74(5): 787–98.
[9] Smouse B, Nikanorov A, La Flash D. Biomechanical forces in the femoropopliteal arterial segment. Endovasc Today 2005;4(6):60–6.
[10] Cheng CP, Wilson NM, Hallett RL, Herfkens RJ, Taylor CA. In vivo MR angiographic quantification of axial and twisting deformations of the superficial femoral artery resulting from maximum hip and knee flexion. J Vasc Interv Radiol 2006;17(6):979–87.
[11] Early M, Kelly DJ. The consequences of the mechanical environment of peripheral arteries for Nitinol stenting. Med Biol Eng Comput 2011;49:1279–88.
[12] Harvey SM. Nitinol stent fatigue in peripheral artery subjected to pulsatile and articulation loading. J Mater Eng Perform 2011:1–9.
[13] Meoli A, Dordoni E, Petrini L, Migliavacca F, Dubini G, Pennati G. Computational modelling of in vitro set-ups for peripheral self-expanding Nitinol stents: the importance of stent–wall interaction in the assessment of the fatigue resistance. CVET 2013;4(3).
[14] Early M, Lally C, Prendergast PJ, Kelly DJ. Stresses in peripheral arteries following stent placement: a finite element analysis. Comput Methods Biomech Biomed Eng 2009;12(1):25–33.
[15] Zhao S, Gu L, Froemming SR. Performance of self-expanding Nitinol stent in a curved artery: impact of stent length and deployment orientation. J Biomech Eng 2012;134(7), 071007.1–071007.6.
[16] Laird JR, Dawson DL. The role for cryoplasty in the treatment of infrainguinal artery disease: case studies. J Endovasc Ther 2009;16(Suppl. II):II116–28.
[17] Vavrik J, Rohrmoser GM, Madani B, Ersek M, Tscholakoff D, Bucek RA. Comparison of MR angiography versus digital subtraction angiography as a basis for planning treatment of lower limb occlusive disease. J Endovasc Ther 2004;11:294–301.
[18] Müller-Hülsbeck S, Schäfer PJ, Charalambous N, Yagi H, Heller M, Jahnke T. Comparison of second-generation stents for application in the superficial femoral artery: an in vitro evaluation focusing on stent design. J Endovasc Ther 2010;17(6):767–76.
[19] Nikanorov A, Smouse HB, Osman K, Bialas M, Shrivastava S, Schwartz LB. Fracture of self-expanding Nitinol stents stressed in vitro under simulated intravascular condition. J Vasc Surg 2008;48:435–40.
[20] Ganguly A, Simons J, Schneider A, Keck B, Bennett NR, Herfkens RJ, et al. In vivo imaging of femoral artery Nitinol stents for deformation analysis. J Vasc Interv Radiol 2011;22(2):244–9.
[21] Pelton AR. Nitinol fatigue: a review of microstructures and mechanisms. J Mater Eng Perform 2011;20:613–7.
[22] Kleinstreuer C, Li Z, Basciano CA, Seelecke S, Farber MA. Computational mechanics of Nitinol stent grafts. J Biomech 2008;41:2370–8.
[23] Petrini L, Wu W, Dordoni E, Meoli A, Migliavacca F, Pennati G. Fatigue behaviour characterization of Nitinol for peripheral stents. Funct Mater Lett 2012;5(1), 1250012.1–1250012.4.
[24] Liu Y, Van Humbeeck J. On the damping behaviour of NiTi shape memory alloy. J Phys 1997;C5:519–24.
[25] Liu Y, Xie Z, Van Humbeeck J, Delaey L. Asymmetry of stress–strain curves under tension and compression for NiTi shape memory alloys. Acta Mater 1998;46(12):4325–38.
[26] Perry KE, Labossiere PE, Steffler E. Measurement of deformation and strain in Nitinol. Exp Mech 2007;47:373–80.
[27] Azaouzi M, Makradi A, Belouettar S. Deployment of self-expanding stent inside an artery: a finite element analysis. Mater Des 2012;41:410–20.
[28] Nematzadeh F, Sadrnezhaad SK. Effects of material properties on mechanical performance of Nitinol stent designed for femoral artery: finite element analysis. Scientia Iranica 2012;19:1564–71.
[29] Pant S, Bressloff NW, Limbert G. Geometry parameterization and multidisciplinary constrained optimisation of coronary stents. Biomech Model Mechanobiol 2011;11:61–82.
[30] Prendergast PJ, Lally C, Daly S, Reid AJ, Lee TC, Quinn D, et al. Analysis of prolapse in cardiovascular stents: a constitutive equation for vascular tissue and finite element modeling. J Biomech Eng 2003;125:692–9.
[31] Loree HM, Grodzinsky AJ, Park SY, Gibson LJ, Lee RT. Static circumferential tangential modulus of human atherosclerotic tissue. J Biomech 1994;27(2):195–204.
[32] Yang Z, Zang HP, Marder M. Dynamics of static friction between steel and silicon. Proc Natl Acad Sci USA 2008;105(36):13264–8.
[33] Park CH, Tijing LD, Pant HR, Kim TH, Amarjargal A, Kim HJ, et al. Accelerated in vitro durability testing of nonvascular Nitinol stents based on the electrical potential sensing method. Appl Phys A 2013;112:919–26.
[34] Pelton AR, Schroeder V, Mitchell MR, Gong XY, Barney M, Robertson SW. Fatigue and durability of Nitinol stents. J Mech Behav Biomed Mater 2008;I:153–64.
[35] Morlacchi S, Migliavacca F. Modeling stented coronary arteries: where we are, where to go. Ann Biomed Eng 2012:1–17.
[36] Nakazawa G, Finn AV, Vorpahl M, Ladich E, Kutys R, Balazs I, et al. Incidence and predictors of drug-eluting stent fracture in human coronary artery a pathologic analysis. J Am Coll Cardiol 2009;54:1924–31.
[37] Papayannis AC, Brilakis ES. Stent fracture: broken stents–broken hearts. Catheter Cardiovasc Interv 2011;78:1106–7.
[38] Holzapfel GA, Sommer G, Gasser CT, Regitnig P. Determination of layer-specific mechanical properties of human coronary arteries with nonatherosclerotic intimal thickening and related constitutive modeling. Am J Physiol-Heart and Circ Physiol 2005;289:H2048–58.
[39] Kelly-Arnold A, Maldonado N, Laudier D, Aikawa E, Cardoso L, Weinbaum S. Revised microcalcification hypothesis for fibrous cap rupture in human coronary arteries. Proc Natl Acad Sci USA 2013;110(26):10741–6.
[40] Runciman A, Xu D, Pelton AR, Ritchie RO. An equivalent strain Coffin–Manson approach to multiaxial fatigue and life prediction in superelastic Nitinol medical devices. Biomaterials 2011;32:4987–93.